

EFFECTS OF THE INCIDENCE ANGLE AND SURFACE TYPE ON THE LIDAR INTENSITY VALUE

Yu-Tien Wu¹ and Chi-Kuei Wang²

¹Graduate student, Department of Geomatics, National Cheng-Kung University

No.1, University Rd., East Dist., Tainan City 701, Taiwan, E-mail: jensh920425@hotmail.com

²Associate Professor, Department of Geomatics, National Cheng-Kung University

No.1, University Rd., East Dist., Tainan City 701, Taiwan, E-mail: chikuei@mail.ncku.edu.tw

KEY WORDS: Rahman-Pinty-Verstraete Model, Bidirectional Reflectance Distribution Function, Bidirectional Reflectance Factor

ABSTRACT: Light Detection and Ranging is an active system, that measures distance by emitting a laser beam to the ground surface and then receiving the reflected signal. The incident angle of the laser beam and the surface type, in addition to its range and atmospheric effects, affect the received signal. Recent studies have utilized the intensity information of airborne LiDAR data for classification. However, such information was not fully explored because these studies only employed single flight lines. Typical airborne LiDAR data consist of multiple flight lines with varying overlaps (40%–60%); this condition implies that a significant portion of the ground objects can be measured from two different viewing aspects (each from adjacent flight lines). The intensity measurements obtained from different viewing aspects can be utilized to exploit the bi-directional reflectance distribution function property of the ground surface for classification. We employed the Rahman–Pinty–Verstraete model to investigate the effects of incident angle and surface type on intensity data, which were obtained with an Optech ALTM Pegasus airborne laser scanner with 60% overlap.

INTRODUCTION

Incidence angle influences the illuminating energy impinged on the surface; these two have a cosine function relationship (Höfle and Pfeifer, 2007; Jutzi and Stilla, 2006). Different surface types have different Bidirectional Reflectance Distribution Function (BRDF); thus, the received energy and incident angle must be obtained with another model (Höfle and Pfeifer, 2007). The Rahman–Pinty–Verstraete (RPV) model, which can describe the relationship between received energy and incident angle, employs three parameters to quantify BRDF (Rahman et al., 1993). The three parameters can describe the shape of BRDF (i.e., concave or convex) and the hot spot effect. Promising results have been obtained from passive remote sensing images, where the full BRDF information simplified by the three parameters of the RPV model is utilized for classification (Koukal and Atzberger, 2012). A few studies have explored the use of full BRDF information for Light Detection and Ranging (LiDAR) data (Disney et al., 2009).

A high degree of overlap is the condition for using the RPV model. Passive remote sensing is applicable because the optical speed of the imaging sensor is sufficiently high to obtain images. The forward overlap can reach 80%–

90%. Currently, most LiDAR data are collected with 40%–60% side overlap because of the constraint imposed by the cost and design of data acquisition. An increasing amount of LiDAR systems is being manufactured with improved capability (e.g., multi-sensors with different viewing angles). The Optech ALTM Pegasus airborne laser scanner has two channels with a 2.2° angle difference. It can obtain more incident angles of the surface because of the high forward overlap. LiDAR system can not only control the light source and emitting energy but also avoids some influencing factors of the passive remote sensing system, such as background reflections and shadows. However, the intensity of received LiDAR data remains affected by incident angle and surface type (Koukal et al., 2014; Kukko et al., 2008). We employed the RPV model to describe the relationship between incident angle and intensity data on different surface types.

MATERIAL

The study area is in Tseng-Wen Reservoir which is located in southern Taiwan (23° 17' 56" N, 120° 39' 56" E) (Figure 1). The LiDAR data were obtained with the Optech ALTM Pegasus airborne laser scanner on July 23 to 24, 2013. The sensor was configured to acquire data with ±9° field of view (FOV). The laser scanner has two different laser channels; the incident angles are 0° and 2.2° in the forward direction. Typical airborne LiDAR data consist of varying overlaps (60%–70%), which implies that a significant portion of the ground objects can be measured from three different viewing aspects. The airborne LiDAR system has an average flying height of 1920 m and point density of 22 points/m². Five consecutive flight lines were selected (flight line numbers 10 to 14; Figure 1(a)) because these five flight lines contain more different surface types. Thirty sample plots were selected. The region contains four surface types, including road, bare land, grass, and roof. The area of the sample plots ranged from 12 m² to 80 m² with the target varying (Figure 1(b)).

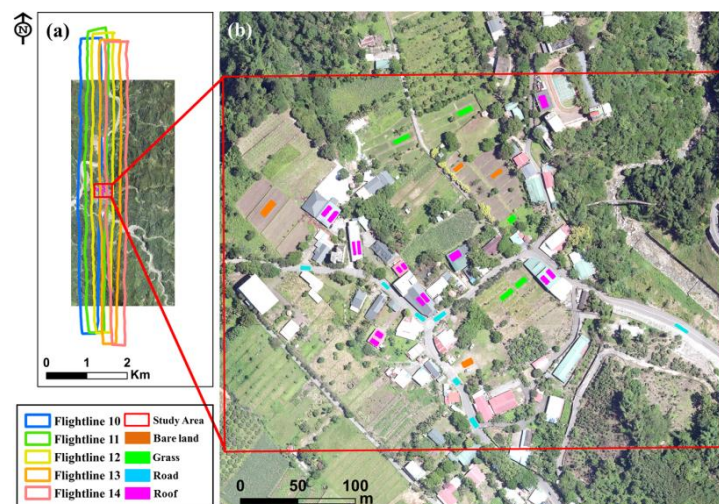


Figure 1. (a) Study area is enclosed in a red box. The distribution of five flight lines is also shown. (b) A total of 30 sample plots containing four surface types each are represented by different color blocks.

METHODOLOGY

The Rahman–Pinty–Verstraete (RPV) model

The BRDF was first proposed by Nicodemus et al. (1977). It describes the light rays reflected on the surface; the light ray incidents on it are from a particular direction. We utilized the RPV model to describe the BRDF. The RPV model is a semi-empirical model (1) that describes surface bidirectional reflectance (Rahman et al., 1993). It doesn't require a rigorous hypothesis on the nature and structure of the surface. Owing to this characteristic, the model can be applied to an actual surface regardless of how complex its structure and type are. Another property of the model is that the parameters utilized are quantitative; the model only requires three parameters to operate (ρ_0, k, θ).

$$\rho_{RPV}(\theta_i, \phi_i, \theta_r, \phi_r) = \rho_0 \cdot \frac{\cos^{k-1}\theta_i \cos^{k-1}\theta_r}{(\cos\theta_i + \cos\theta_r)^{1-k}} \cdot F(g) \cdot [1 + R(G)] \quad (1)$$

where ρ_{RPV} is the reflectance of a surface illuminated from direction (θ_i, ϕ_i) to observed direction (θ_r, ϕ_r) , ρ_0 is an arbitrary parameter that characterizes the intensity of the reflectance of the surface ($0 \leq \rho_0 \leq 1$), and k indicates the level of anisotropy of the surface ($k < 1$ for the bowl-shaped pattern, $k > 1$ for the bell-shaped pattern).

The second term of the RPV model (1) is modified by the Minnaert function (Minnaert, 1941). The other components of the RPV model are shown below. The function $F(g)$ is

$$F(g) = \frac{1 - \theta^2}{[1 + \theta^2 - 2\theta \cdot \cos(\pi - g)]^{1.5}} \quad (2)$$

where θ is the parameter that controls the relative amount of forward ($0 \leq \theta \leq 1$) and backward ($-1 \leq \theta \leq 0$) scattering. The phase angle of scattering g is provided by

$$\cos(g) = \cos\theta_i \cos\theta_r + \sin\theta_i \sin\theta_r \cos(\phi_i - \phi_r) \quad (3)$$

The hot spot effect is approximated by :

$$1 + R(G) = 1 + \frac{1 - \rho_0}{1 + G} \quad (4)$$

where G is the geometric factor provided by

$$G = [\tan^2\theta_i + \tan^2\theta_r - 2 \cdot \tan\theta_i \tan\theta_r \cos(\phi_i - \phi_r)]^{0.5} \quad (5)$$

The application of the RPV model

The RPV parameters and incident angle were varied to understand how they affect the RPV model values. All the

variations are shown in Figure 2. The parameters in Figure 2(a) were used as reference guideline to compare with other parameters. The magnitude of the model results varied with ρ_0 , and shape patterns were controlled by k sensitivity. The orientation of the hot spot effect varied as the θ value changed. This condition is similar to the conditions when the RPV model is used in LiDAR intensity in Figure 2 (right column).

The intensity of the LiDAR point clouds is mainly due to backscattering because the incident angle of the beam is equal to the angle of reflection. The azimuth angle of the incident and reflected beam is assumed to be 0 degrees. Based on the above condition, the simplified formula of the RPV model used in LiDAR is provided by

$$\rho_{RPV}(\theta_i) = \rho_0 \cdot \frac{\cos^{2k-2}\theta_i}{(2\cos\theta_i)^{1-k}} \cdot \frac{1-\theta^2}{[1+\theta^2+2\theta]^{1.5}} \cdot [2 - \rho_0] \quad (6)$$

Examples of the results of this formula are shown on the right side of Figure 2. In addition to ρ_0 affecting the magnitude of the models (Figures 2(a) and 2(b)), parameter k varied from 1.25 (> 1) to 0.9 (< 1); the models exhibited a bowl-shaped pattern from its initial bell-shaped one (Figures 2(a) and 2(c)). When θ was changed from -0.5 to 0.5 , the value of the models decreased considerably because of positive θ , which indicates that forward scattering is mainly for the data and backward scattering is minimal (Figures 2(a) and 2(d)). We employed the simplified RPV model to fit the actual LiDAR data and determine the relation between incident angle and intensity. The parameters were estimated according to the fitting result.

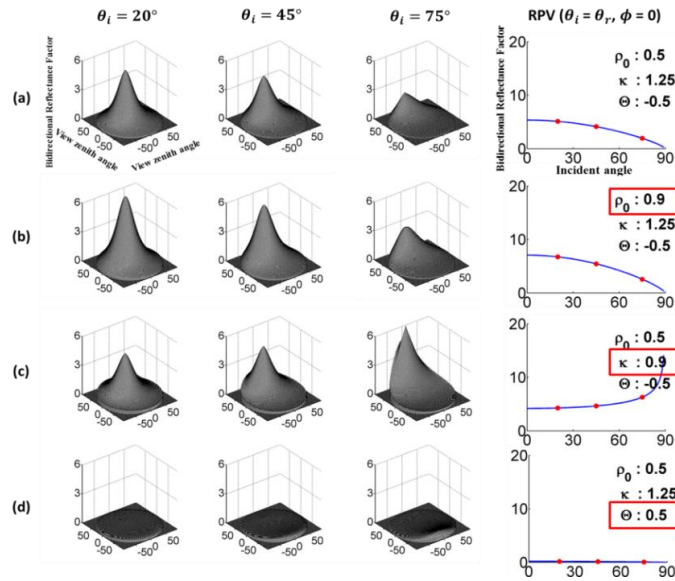


Figure 2. Examples of varying the three parameters (ρ_0 , k , θ) are shown in (b) to (d). (a) is for reference. Three cases of incident angles are shown. The RPV model used in the LiDAR condition and each parameter value of the models are shown in the rightmost figure. The red box shows the varied parameter.

RESULTS AND DISCUSSION

The fitting results of the RPV parameters are shown in Figure 3. The results of parameter θ are negative for all feature types and thus indicate the dominance of backward scattering because of the fact that the LiDAR data are

retroreflective. The dominance of backward scattering is slightly higher for grass than for other types, because its θ value is higher in the former. The parameter k of bare land is lower than that of grass and road. Roof shows considerable variation in k but not so much in ρ_0 and θ . Parameter ρ_0 and θ of all surface types appear to have a symmetrical trend.

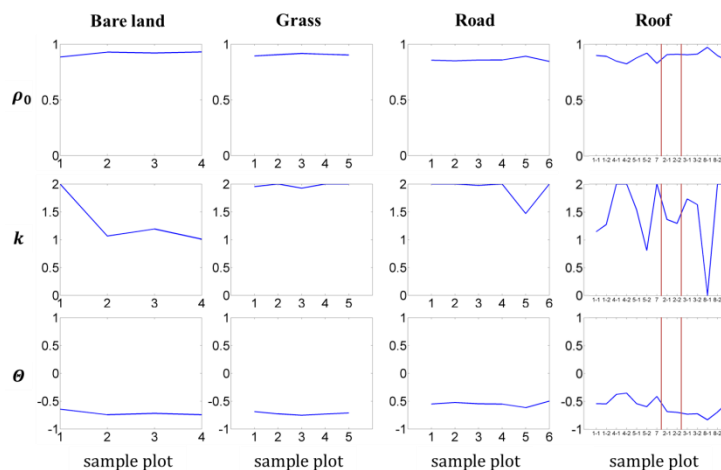


Figure 3. RPV parameters derived from the fitting results of all sample plots containing four surface types.

The relation of RPV-modelled incident angle and intensity show specific class differences for the selected sample plots (bare land, grass, road and roof). This relation is analyzed by visual and qualitative analysis in Figure 4. The bare land and road fitting curves are close to straight lines and more concentrated, but the road curves tend to be slightly oblique. The distributions of grass fitting curves are more separate and bended than those of bare land and road probably because of the different generation times of grass. The fitting curve of bare land is relatively flat and is agreement with the foregoing result that parameter k of bare land is lower than that of grass and road. Through aerial photographs, the type of roof materials can be divided into four categories (Figure 4(d)) (the roof types are separated by red lines). The roof fitting curves results are also grouped into four types according to the magnitude of the difference among the intensity values in Figure 4(d). Except for inclined roof, the LiDAR incident angle of the surface types are concentrated below 20 degrees, given that FOV was set between -9° – 9° .

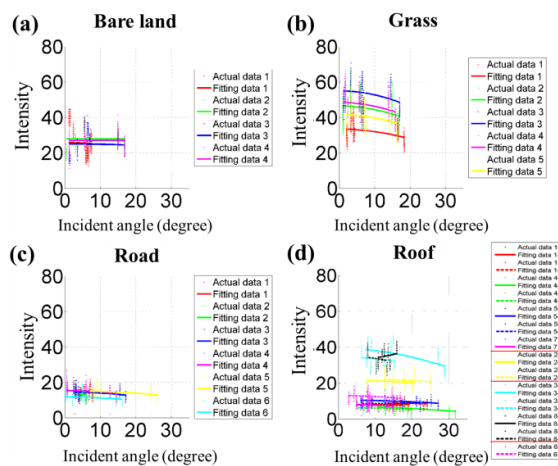


Figure 4. Fitting results of the four surface types.

CONCLUSION

This study investigated the effect of incident angle and surface type on LiDAR intensity and evaluated the feasibility of using the semi-empirical RPV model for LiDAR data. Different surface features can be distinguished by RPV parameters. Bare land and road exhibit a common trend with high consistency; however, grass shows a common trend with a large variation. In addition, the parameter θ in all the sample plots is negative, which is consistent with the LiDAR data property when the receiver is placed in the retroreflection direction. Parameters ρ_0 and θ are similar in the different surface types, but parameter k is different. The promising results of the RPV show that the model can be applied to LiDAR data.

REFERENCES

- Disney, M.I., Lewis, P.E., Bouvet, M., Prieto-Blanco, A., Hancock, S., 2009. Quantifying Surface Reflectivity for Spaceborne Lidar via Two Independent Methods. *Ieee T Geosci Remote* 47, pp. 3262-3271.
- Höfle, B., Pfeifer, N., 2007. Correction of laser scanning intensity data: Data and model-driven approaches. *ISPRS Journal of Photogrammetry and Remote Sensing* 62, pp. 415-433.
- Jutzi, B., Stilla, U., 2006. Range determination with waveform recording laser systems using a Wiener Filter. *ISPRS Journal of Photogrammetry and Remote Sensing* 61, pp. 95-107.
- Koukal, T., Atzberger, C., 2012. Potential of Multi-Angular Data Derived From a Digital Aerial Frame Camera for Forest Classification. *Selected Topics in Applied Earth Observations and Remote Sensing, IEEE Journal of* 5, pp. 30-43.
- Koukal, T., Atzberger, C., Schneider, W., 2014. Evaluation of semi-empirical BRDF models inverted against multi-angle data from a digital airborne frame camera for enhancing forest type classification. *Remote Sensing of Environment*.
- Kukko, A., Kaasalainen, S., Litkey, P., 2008. Effect of incidence angle on laser scanner intensity and surface data. *Appl. Opt.* 47, pp. 986-992.
- Minnaert, M., 1941. The reciprocity principle in lunar photometry. *Astrophys J* 93, pp. 403-410.
- Nicodemus, F.E., Richmond, J.C., Hsia, J.J., Ginsberg, I.W., Limperis, T., 1977. *Geometrical Considerations and Nomenclature for Reflectance*. U.S. Government Printing Office.
- Rahman, H., Pinty, B., Verstraete, M.M., 1993. Coupled surface-atmosphere reflectance (CSAR) model. II: Semiempirical surface model usable with NOAA advanced very high resolution radiometer data. *Anglais* 98, pp. 20,791-720,801.